Salim Ok*, Julie Sheets, Susan A. Welch, David R. Cole,
Marc Berman, Armando Rúa, Steve Greenbaum,
Deepansh J. Srivastava and Philip J. Grandinetti

# High-temperature and high-pressure NMR investigations of low viscous fluids confined in mesoporous systems

https://doi.org/10.1515/zpch-2019-1510
Received July 2, 2019; accepted June 23, 2020; published online September 24, 2020

**Abstract:** In this contribution, the relaxation and diffusional behaviors of low viscous fluids, water and methanol confined into mesoporous silica and controlled size pore glass were investigated. The engineered porous systems are relevant to geologically important subsurface energy materials. The engineered porous proxies were characterized by Brunauer–Emmett–Teller (BET) surface analyzer, nuclear magnetic resonance (NMR) spectroscopy, and electron microscopy (EM) to determine surface area, pore-wall protonation and morphology of these materials, respectively. The confined behavior of the low viscous fluids was studied by varying pore diameter, fluid-to-solid ratio, temperature, and pressure, and then compared to bulk liquid state. Both relaxation and diffusion behaviors for the confined fluids showed increasing deviation from pure bulk fluids as the fluid-to-solid ratio was decreased, and surface-to-volume ratio ($S/V$) was varied. Variable pressure deuteron NMR relaxation of confined $D_2O$ and confined methanol, deuterated at the hydroxyl or methyl positions, were performed to exploit the sensitivity of the deuteron quadrupole moment to molecular rotation. The methanol results demonstrated greater pressure dependence than those for water only in bulk. The deviations from bulk liquid behavior arise from different reasons such as confinement and the interactions between confined fluid and the nano-pore

***Corresponding author: Salim Ok**, School of Earth Sciences, The Ohio State University Columbus, Columbus, Ohio 43210, USA, E-mail: sok@uos.de
**Julie Sheets and Susan A. Welch:** School of Earth Sciences, The Ohio State University, Columbus, Ohio 43210 USA
**David R. Cole:** School of Earth Sciences, The Ohio State University, Columbus, Ohio 43210 USA; and Department of Chemistry, The Ohio State University, Columbus, Ohio 43210, USA
**Marc Berman, Armando Rúa and Steve Greenbaum:** Department of Physics & Astronomy, Hunter College of the City University of New York, New York, NY 10065, USA
**Deepansh J. Srivastava and Philip J. Grandinetti:** Department of Chemistry, The Ohio State University, Columbus, Ohio 43210, USA

wall. The results of the present report give insight into the behavior of low viscosity fluid in nano-confined geometries under different state conditions.

**Keywords:** confined state; diffusion; high-pressure NMR; low viscous fluids; relaxation.

# 1 Introduction

The behavior of even simple, low viscous fluids such as water and methanol in confined geometries can differ markedly from bulk behavior [1–4] in several ways because of the effects of large internal surfaces and geometrical confinement, respectively. Phase transitions (i.e., freezing and capillary condensation), sorption and wetting, and dynamical behaviors, including diffusion and relaxation, may be adapted, with the strongest alterations detected for pores ranging from <2 to 50 nm—the micro- and mesoporous regimes [5, 6]. A number of factors including the size, shape, distribution, and interconnectedness of confined geometries, the character of the liquid–surface interaction (i.e., chemistry of the fluids of interest and solid), and their physical properties order how fluids, and with them reactants and products of intrapore transformations, move around and through these nano-environments, wet, and ultimately adsorb and react with the solid surfaces [7, 8]. Additionally, the effects of elevated temperature and/or pressure common to earth sciences and certain engineered catalytic process systems can have a significant role in further altering the structure and dynamics of fluid behavior on wetted surfaces or in confined volumes. Due to the complexity of natural C–O–H-fluids and their roles in intervening surface interactions and reactivity with mineral phases, it is for sure that a quantitative clarification of molecular-level fluid properties and fluid interactions with solids is needed. The development of advanced synthesis and characterization methods for micro- and mesoporous solids allowed varying pore structure and sizes of the engineered proxies as well [9].

Among various techniques to characterize the nanoporous engineered proxies and to study confined fluid behavior, nuclear magnetic resonance (NMR) spectroscopy is a non-invasive one that allows studying the geometry of the porous materials [10]. NMR spectroscopy describes and classifies the sub-surfaces and assembly of the porous spaces in nanometer scales, and hence gives insight in how fluids are confined into the nanopores and how the confined fluid molecules move within the nanoporous media [11]. Measuring the variations in diffusive and relaxation activities with respect to bulk state by boundaries where particles reside permits obtaining information directly related to the basic properties of the

nanopore space [11–13]. For example, D'Orazio and co-workers filled the porous silica material with various amounts of distilled water and assessed diffusion via pulsed field gradient (PFG) NMR and NMR relaxation measurements. Finding linear behavior of both longitudinal ($T_1$) and transverse ($T_2$) relaxation measurements with respect to the degree of fluid filling down to monolayer coverage was explained by the homogeneity of pore space forming uniform distribution of water [14–16]. However, porous silica is a heterogeneous material with –OH groups on silica surface as found by solid-state magic angle spinning (MAS) cross-polarization (CP) NMR [17, 18]. It was also shown that water molecules near the interface had preferred orientations because of the interaction with –OH groups on the surface of nano-porous silica [19].

The necessity of studying confined fluids inside nano-porous materials comes from the contradictory conclusions regarding the impact of confinement on fluid behavior. D'Agostino and co-workers [3] observed that diols such as ethylene glycol and 1,2-propanediol showed increased diffusivity within the pore space of titania and silica relative to alkanes including *n*-hexane and *n*-octane. $T_1$ measurements for $^1$H also demonstrated that tumbling rate of polyols is not influenced by the porous medium while the drop of $T_1$ for the alkanes was significant. Confining water in one or two dimensions resulted in new and controversial conclusions in both experimental [20–22] and computational studies [23, 24].

The objective is to probe the molecular- to microscopic-level behavior of the low viscous fluids confined within mesoporous engineered materials that one may also consider a reasonable proxy for natural earth phases. We explored the behavior of fluids as a function of a number of key parameters including but not limited to pore size, pore volume, fluid type, fluid-to-solid ratio, temperature and pressure. Mesoporous silica ($SiO_2$) having 200 nm particle size and 4 nm pore size, and controlled size pore glass with 35 nm pore diameter were used as subsurface model systems for exploring nano-confinement behaviors of $H_2O$, $CH_3OH$ and their deuterated versions.

First, we focused on a thorough and careful analysis of the nanoporous materials by solid-state CP MAS $^{29}$Si NMR, BET gas adsorption and both scanning and transmission electron microscopy techniques. Second, both PFG NMR, and more sensitive $T_1$ NMR measurements were conducted to quantify dynamical behavior of water and methanol under confinement.

In performing $T_1$ NMR measurements, fluid-to-solid ratio was the first variable to have the following samples: (i) partially filled nanoporous solids, (ii) nanoporous solids filled completely, and (iii) nanoporous matrices filled completely but with excess fluid. Confined fluid behavior is studied by varying the temperature with the goals of assessing the temperature effect of the fluid as temperature approaches the boiling point, and testing whether the porous materials remain

stable at elevated temperatures. The other focus of the study is the high-pressure $^{2}H$ NMR relaxation investigation of fluids under confinement. Water and methanol, and their deuterated forms exhibit hydrogen-bonding characteristics, and bulk water is not compressible under high-pressure over the range used in this investigation while bulk methanol is slightly compressible. The high-pressure NMR approach affords the opportunity to test the potential role of compressibility of the two fluids under confinement and explore the deviation from bulk behavior under geochemically relevant high-pressure conditions. Additional diffusion NMR measurements were conducted with partially filled pores without excess fluid to investigate the translational attitude of the confined fluids and the deviation of confined fluid from corresponding bulk behavior.

# 2 Experimental details

## 2.1 Chemicals, materials and basic characterization

Mesoporous silica (200 nm average particle size and 4 nm average pore size) and controlled pore glass (35 nm average pore size) were purchased from Sigma-Aldrich. Herein, we will use the two following abbreviations for distinguishing the two porous materials: silica-4 nm, and cpg-35 nm. Deuterated solvents were provided by Sigma-Aldrich with 99.9% purity. BET surface area, pore volume and pore diameter of the engineered silica were measured with nitrogen adsorption and desorption in liquid $N_2$ with a Micromeritics, ASAP 2020 surface area and porosity analyzer (see Supplementary Table S1). Before running the adsorption–desorption measurements, the samples were degassed at 150 °C for 20 h under a vacuum pressure of 10 μmHg.

Both morphology and pore structure of the mesoporous silica (Supplementary Figure S1 (a–b)) were studied by scanning and transmission electron microscope, using an FEI Quanta 250 field emission gun SEM, and FEI Titan3 80–300 kV TEM, respectively, whereas the morphology of the controlled pore glass was only examined by scanning electron microscopy, utilizing an FEI Quanta 250 field emission gun SEM (Supplementary Figure S1 (c)). Small quantities of the silica powders (without pre-treatment or grinding) were deposited on carbon tape mounted on aluminum stubs, and then lightly coating with Au/Pd using a Denton Desk V sputter coater for SEM measurements. In order to prepare the samples for TEM measurements, (5–10 mg) of the silica powders were ultra-sonicated in water, followed by dispersing the suspensions on carbon film supported 200 mesh copper grids. TEM grids were lightly covered with Au/Pd. The samples were then measured in bright field mode at an accelerating ion voltage of 300 kV. The

mesoporous silica has spherical morphology, as shown in Figure S1 (a). The TEM image (Figure S1 (b)) of the same engineered system shows superstructure with approximately 4 nm pores in a parallel array [25]. SEM images of cpg-35 nm reveal that this synthetic system exhibits pores with a network type structure.

## 2.2 NMR spectroscopy

### 2.2.1 Pore wall chemistry

In order to characterize the surface hydroxyl species, $^{29}$Si solid-state NMR experiments were performed using Bruker 400 MHz (9.4 T) spectrometer operating at radio frequencies of 79.5 and 400 MHz for $^{29}$Si and $^{1}$H, respectively. Both $^{29}$Si direct polarization (DP) and $^{1}$H/$^{29}$Si cross-polarization (CP) magic-angle spinning (MAS) pulse sequence were modified to accommodate echo train acquisition for enhanced signal sensitivity. The experiments were conducted with a 7 mm (outer diameter rotor) Bruker MAS NMR probe. The direct polarization spectra were recorded at a spinning frequency of 5 kHz with 600 s recycle delay and 120 echoes and averaged over 128 scans, while the CP MAS spectra were acquired at spinning frequency of 5 kHz with 1.3 s recycle delay and 50 echoes averaged over 6144 scans. The CP/MAS spectra accentuate the existence of surface –OH groups of the nanoporous silica systems.

Even though the silica systems are generally described as $SiO_2$, it is well known that such silica systems are water absorbing [17]. For this reason, there are three Q sites in the vicinity of and further apart from Si sites (Supplementary Figure S2 (a–f)). The Q sites are as follows: Q(2)-geminal-hydroxyl silanol sites $(>SiO)_2Si(OH)_2$, Q(3) – the single hydroxyl silanol sites $(>SiO)_3SiOH$, and Q(4) – the surface silicon atoms of the $(>SiO)_4Si^*$ type [17, 26]. The presence of –OH on the surface of the silica at the Q(2) and Q(3) sites means the silica is indeed heterogeneous, and as such, more realistic to what is observed in both natural as well as engineered systems (see detailed explanation about heterogeneity of silica-4.0 nm in Supplementary Information).

### 2.2.2 Low fluid volume NMR experiments

Measurements on low fluid-to-solid ratio systems were performed on a 300 MHz NMR magnet for Varian direct digital drive solid state NMR system using a DOTY Z-Spec Diffusion probe. Table 1a summarizes the experimental conditions (fluid-solid ratio, temperatures, etc.), while Table 1b and Table 1c give the amount of confined and excess fluid content of the nanoporous systems in terms of number of

**Table 1a:** Experimental conditions.

| Instrument | Measurements | Variable | Fluid type | Nanoporous matrix | Number of fluid/solid ratio |
|---|---|---|---|---|---|
| (1) 300 MHz[a] | Longitudinal relaxation | Pore diameter, fluid/solid ratio, fluid chemistry | $D_2O$, $CD_3OD$ | Silica-4 nm; cpg-35 nm | 4 |
| (2) 300 MHz[a] | Longitudinal relaxation | Temperature | $CD_3OD$ | Silica-4 nm | 1 |
| (3) 300 MHz[a] | Longitudinal relaxation | Pore diameter, temperature, fluid chemistry | $\boldsymbol{CD_3}OH$, $CH_3\boldsymbol{OD}$ | Silica-4 nm; cpg-35 nm | 1 |
| (4) 300 MHz[a] | Longitudinal relaxation | Pore diameter, temperature, fluid/solid ratio, fluid chemistry | $\boldsymbol{CD_3}OH$, $CH_3\boldsymbol{OD}$ | silica-4 nm; cpg-35 nm | 3 |
| (5) 300 MHz[a] | Longitudinal relaxation | Temperature, pore diameter | $D_2O$ | Silica-4 nm; cpg-35 nm | 1 |
| (6) 300 MHz[b] | Longitudinal relaxation | Pressure, fluid/solid ratio | $D_2O$ | Silica-4 nm; cpg-35 nm | 2 + 3 |
| (7) 300 MHz[b] | Longitudinal relaxation | Pressure, fluid/solid ratio | $CD_3OD$ | Silica-4 nm; cpg-35 nm | 2 + 2 |
| (8) 300 MHz[a] | Diffusion | Pore diameter, fluid/solid ratio | $H_2O$ | Silica-4 nm; cpg-35 nm | 4 |
| (9) 300 MHz[a] | Diffusion | Pore diameter, fluid/solid ratio | $CH_3OH$ | Silica-4 nm; cpg-35 nm | 3 |

| Instrument | Measurements | Fluid/Solid Ratio | Temperature | Figure Number |
|---|---|---|---|---|
| (1) 300 MHz[a] | Longitudinal relaxation | 0.20 ml; 0.10 ml; 0.05 ml; 0.02 ml/0.050 g | 298 | 1 (a–b) |
| (2) 300 MHz[a] | Longitudinal relaxation | 0.10 ml/0.050 g | 298; 308; 318; 328 | 2 (a–b) |
| (3) 300 MHz[a] | Longitudinal relaxation | 0.10 ml/0.050 g | 298; 308; 318; 328 | 2 (c–d) |
| (4) 300 MHz[a] | Longitudinal relaxation | 0.10 ml; 0.05 ml; 0.02 ml/0.050 g | 298; 308; 318; 328 | 3 (a–d) |
| (5) 300 MHz[a] | Longitudinal relaxation | 0.07 ml/0.050 g | 298; 308; 318; 328 | 5 |
| (6) 300 MHz[b] | Longitudinal relaxation | Values given on Figure 6a | 298 | 6 (a) |
| (7) 300 MHz[b] | Longitudinal relaxation | Values given on Figure 6b | 298 | 6 (b) |
| (8) 300 MHz[a] | Diffusion | 0.20 ml; 0.10 ml; 0.05 ml; 0.02 ml/0.050 g | 298 | 7 (a) |
| (9) 300 MHz[a] | Diffusion | 0.10 ml; 0.05 ml; 0.02 ml/0.050 g | 298 | 7 (b) |

[a]Varian 300 MHz, static solid probe that allowed lower volume measurements.
[b]Chemagnetics 300 MHz, probe with high-pressure chamber having NMR excitation coil inside.

molecules per specific surface area prepared referring to Grünberg et al. [27]. $^{1}$H NMR experiments used tetramethylsilane (TMS) as a reference whose signal is at 0 ppm whereas $^{2}$H experiments used $D_2O$ at 0 ppm as a reference. $^{2}$H $T_1$ measurements were performed either using a $T_1$ saturation or $T_1$ inversion recovery sequence with recovery periods ranging between 1 ms and 1 min $^{1}$H diffusion measurements were performed utilizing a pulsed field gradient stimulated echo sequence with gradient strengths up to 1300 G/m. Diffusion times were 50 ms and gradient pulse lengths were 2 ms for all measurements. Prior to the measurements, the sample was soaked in the fluid for at least 24 h to make sure that the wetting reached full saturation. Prior to each measurement, samples were sonicated for 5 min to ensure a homogeneous distribution of the fluid. Data were fit using the Bloch equations for $T_1$ and the Stejskal–Tanner equation for diffusion, respectively.

### 2.2.3 High-pressure NMR experiments

High-pressure NMR experiments were conducted on a Chemagnetics 300 MHz spectrometer. For high-pressure measurements (up to 250 MPa), the samples were hermetically sealed in thin polyethylene bags with a negligible proton NMR background signal with respect to the liquid signal. The fluid-to-solid ratio was changed from higher values to lower ones. Accurate manipulation of the pressure was completed utilizing an ENERPAC 11-400 hydraulic system fitted to a sealed Cu–Be alloy high-pressure chamber (bomb) inside of which the NMR excitation coil and sample are located. The pressure-transmitting fluid was a FC-77 Fluorinert (3M), checked for absence of $^{1}$H NMR resonances. $T_1$ values were determined using the well-known inversion recovery pulse sequence.

## 3 Results and discussion

This study provides a unique “window” into the dynamical behavior of two different hydrogenous fluids systematically probed under nano-confinement by varying the wetting degree, temperature, and pressure. Our approach explored how the silica pore walls decorated with –OH groups influence the dynamics of the confined fluids with different hydrogen bonding capability. Further, the selection of nanoporous silicas with completely different geometries (straight channels versus more irregular shapes) provided new insights into the effect of pore geometry, size, and surface area on the molecular relaxation behavior of the confined fluids. Finally, the effect of temperature on both confined fluid behavior and thermal stability of the nano-porous engineered materials were investigated. This

is one of the few studies to assess the compressibility of confined fluids in nano-confinement by high-pressure NMR.

## 3.1 Longitudinal relaxation time of water and methanol

NMR longitudinal relaxation times ($T_1$) is more responsive to the local chemical environment compared to diffusion, and it gives insight into more localized and limited movements such as translational and rotational motions on a time scale similar to the reciprocal of the NMR angular frequency (~1 ns) [28]. $T_1$ is mainly governed by energy, and measures of the dipolar interactions with themselves and the surroundings [28]. The molecular motions contribute to $T_1$ in liquids are (i) dipole–dipole interaction, (ii) spin–rotation interaction, (iii) scalar-coupling, (iv) chemical shift anisotropy, (v) possible interaction because of the existence of some paramagnetic materials in natural substances [29]. Kleinberg et al. argued that nucleus-electron interactions instead of pore dimensions manage the proton relaxation rate of pore-confined fluids in such natural substances [30]. In the current study, the fluids were either partially or completely deuterated. Deuteron has a nuclear spin of 1, and thus a nuclear quadrupolar moment. The deuteron spin $I = 1$ ensures that the relaxation stays modestly exponential in the dispersion zone [31]. The relaxation behavior of deuterated fluids is dominated by electric field gradient fluctuations [32]. In the case of proton $T_1$ relaxation, the protons relax by dipole–dipole interaction. Both intra- and intermolecular interactions contribute to the relaxation rate observed. The deuteron relaxation is dominated by intra-molecular interactions [33]; hence complete relaxation by intramolecular quadrupole interaction particularly reveals data on re-orientational effects [31]. In other words, $T_1$ is governed by dipolar and quadrupolar interactions for $^{1}$H and $^{2}$H, respectively. Moreover, $^{2}$H NMR is mainly appropriate for studying molecular mobility for a number of reasons. The quadrupole coupling constant ($Q_{CC}$) is two orders larger than the proton dipole–dipole coupling in magnitude. Because $Q_{CC}$ relies on deuteron location, it may yield information on the local structure and bonding. Most importantly, the $Q_{CC}$ involves only one spin, the adjacent nuclei does not influence the information on molecular reorientation. In this way, the clear discrimination between possible motions becomes possible due to the motional averaging of the quadrupole interaction [34, 35].

Figure 1a and b indicates the NMR longitudinal relaxation ($T_1$) values of $D_2O$ and $CD_3OD$ in mixtures with cpg-35 nm and silica-4 nm. $T_1$ of $D_2O$ in mixtures with cpg-35 nm did not show any decrease- only below 0.05 ml insignificantly (Figure 1a). (Short description of NMR relaxation theory is given in the Supplementary Information). In the mixtures with silica-4 nm having narrower pores the

**Table 1b:** Water content of the silica-4 nm and cpg-35 nm samples.

| vol (ml) $H_2O$ | Mass (mg)-silica 4 nm | Pore volume of nanoporous matrix (ml) | *n* [($H_2O$) per $nm^2$][a] | vol%[b] | Mass (mg)-cpg 35 nm | Pore volume of nanoporous matrix (ml) | *n* [($H_2O$) per $nm^2$][a] | vol%[b] |
|---|---|---|---|---|---|---|---|---|
| 0.20 | 50 | 0.052 | ***58.2 (surface)*** + ***165.9 (excess)*** | >100 | 50 | 0.045 | ***524 (surface)*** + ***1798.9 (excess)*** | >100 |
| 0.10 | 50 | 0.052 | ***58.2 (surface)*** + ***53.7 (excess)*** | >100 | 50 | 0.045 | ***524 (surface)*** + ***635.7 (excess)*** | >100 |
| 0.07 | 50 | 0.052 | ***58.2 (surface)*** + ***20.2 (excess)*** | >100 | – | 0.045 | – | – |
| 0.05 | 50 | 0.052 | 55.9 | 96.1 | 50 | 0.045 | ***519*** | 99 |
| 0.02 | 50 | 0.052 | 22.4 | 38.5 | 50 | 0.045 | 230.7 | 44 |

[a]The number of $H_2O$ molecules on the surface per $nm^2$ (calculated with respect to the specific surface area).
[b]The content of $H_2O$ in vol% (calculated with respect to the specific pore volume).

**Table 1c:** Methanol content of the silica-4 nm and cpg-35 nm samples.

| vol (ml) $CH_3OH$ | Mass (mg)-silica 4 nm | Pore volume of nanoporous matrix (ml) | *n* [($CH_3OH$) per $nm^2$][a] | vol%[b] | Mass (mg)-cpg 35 nm | Pore volume of nanoporous matrix (ml) | *n* [($CH_3OH$) per $nm^2$][a] | vol%[b] |
|---|---|---|---|---|---|---|---|---|
| 0.20 | 50 | 0.052 | ***25.8 (surface)*** + ***74.0 (excess)*** | >100 | 50 | 0.045 | ***232.6 (surface)*** + ***802.1 (excess)*** | >100 |
| 0.10 | 50 | 0.052 | ***25.8 (surface)*** + ***24.4 (excess)*** | >100 | 50 | 0.045 | ***232.6 (surface)*** + ***284.8 (excess)*** | >100 |
| 0.05 | 50 | 0.052 | 24.9 | 96.5 | 50 | 0.045 | ***232.6 (surface)*** + ***25.7 (excess)*** | ≈100 |
| 0.02 | 50 | 0.052 | 10.1 | 39.1 | 50 | 0.045 | 46.9 | 20.2 |

[a]The number of $CH_3OH$ molecules on the surface per $nm^2$ (calculated with respect to the specific surface area).
[b]The content of $CH_3OH$ in vol% (calculated with respect to the specific pore volume).

decrease was clear even below 0.2 ml. The well-known deviation from bulk behavior upon confinement appeared in the current report as differences in $T_1$ values of the heterogeneous mixtures with respect to those of the pure fluid [36]. Such differences might arise from, for instance, changes in friction coefficient, diffusion constants, etc. For higher fluid-to-solid ratios, the deviation of $T_1$ values from that of bulk was attributed to the molecular interactions dominating the $T_1$.

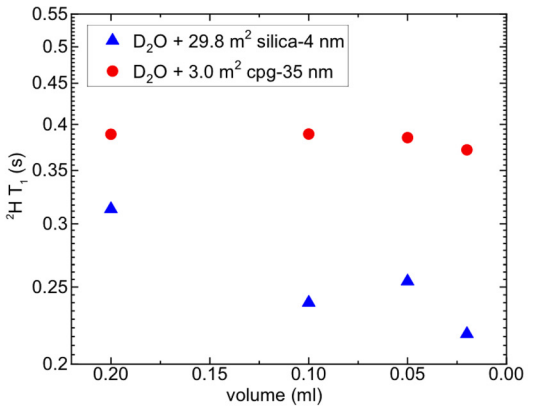


(a)

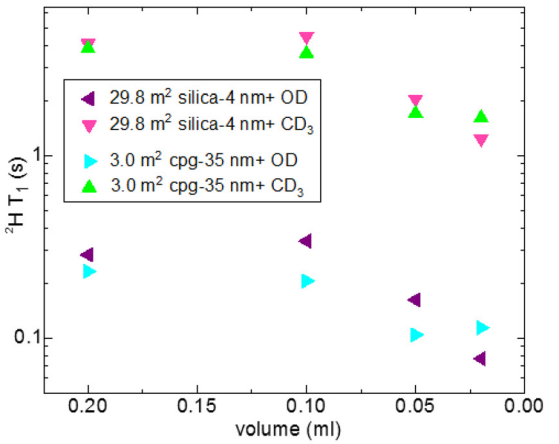


(b)

**Figure 1:** (a, b): (a) $T_1$ of $D_2O$ in mixtures with silica-4 nm and cpg-35 nm as a function of volume at 298 K and where the amount of solid is 0.050 g. (b) $T_1$ of $CD_3OD$ in mixtures with silica-4 nm and cpg-35 nm as a function of volume at 298 K and where the amount of solid is 0.050 g.

However, for lower fluid-to-solid ratios, in addition to the molecular interactions, decrease in diffusion coefficient affected the $T_1$ attitude.

In analyzing the relaxation behavior of deuterated-methanol, there were two signals observed as expected arising from $CD_3$ and OD. Longitudinal relaxation time values of $CD_3$ were higher than those of OD. This was independent of the porous matrix system. Referring to BPP theory, we suggest that this higher $T_1$ value of $CD_3$ with respect to OD is because of rapid $CD_3$ molecular rotation about its symmetry axis (Figure 1b). The $T_1$ values of OD did not show significant variations when the fluid-to-solid ratio was changed. The motion of $CD_3$ was affected only below 0.1 ml. More interestingly, in the case of both of the porous systems, the general relaxation trends of $CD_3$ and OD were independent of pore diameter.

The longitudinal relaxation time measurements with 0.1 ml $CD_3OD$ in the mixture with mesoporous silica were performed at elevated temperatures. Because the boiling point of methanol is 64.7 °C, the measurements were conducted only up to 55 °C. As mentioned above, the $T_1$ time of –OD was shorter than that of $-CD_3$ (Figure 2a and b). Both $CD_3$ and OD exhibited discontinuous $T_1$ temperature dependence rather than $T_1$ minima, showing that molecular motion of the confined fluid molecules governs temperature dependence of $T_1$ [37], stemming from $\tau_c$ of molecular motion. Arrhenius equation describes the temperature dependence even in a discontinuous case of $\tau_c$ as $\tau_c = \tau_0 \exp(E_a/RT)$ where $E_a$ is the activation energy and $\tau_0$ is the pre-exponential factor. We have performed also relaxation measurements ($^2$H-$T_1$) with partially deuterated methanol samples of $CH_3OD$ and $CD_3OH$. Additionally, we deal with deuterated samples, because deuteron spin $I = 1$ ensures that the relaxation occurs exponentially. In Angell's categorization [38, 39], covalently bonded systems with Arrhenius temperature dependence are considered strong. Whereas, some ionic liquids showing highly non-Arrhenius behavior are defined as fragile. The Arrhenius temperature reliance observed in the current study suggests that deuterated fluids in confined state for the given temperature range exhibit strong behavior [40].

The measurements were conducted by varying temperature for the same amount of substrate (50 mg either silica-4 nm or cpg-35 nm) and the same amount of fluid, 0.1 ml methanol (Figure 2c and d). The relaxation values of –OD in the case of $CH_3OD$ wetted samples was slightly lower in mixtures with cpg-35 nm than in nanoporous silica. This result matches the observation shown in Figure 1b. The relatively higher $T_1$ in porous silica means enhanced molecular tumbling arising from disruption in hydrogen bonding network. When the temperature was elevated, the gap between the relaxation values increased. In the case of $CD_3OH$ wetted samples, the relaxation values of $-CD_3$ was higher in mixtures with cpg-35 nm than in silica-4 nm.

Figure 3a and b compares $^2$H-$T_1$ relaxation times. In this case, as the temperature was increased, the difference between the relaxation values decreased. There are two contradictory situations. In order to resolve this, the experiments were tended as a function of other parameters. First, as the ratio of the amount of fluid to the wetted surface area was decreased, the relaxation decreases. This correlation was independent of pore size. As the temperature was elevated, the relaxation times also increased. The $-CD_3$ relaxation time was longer than that of the –OD group. When we compare the deuteron relaxation time of $-CD_3$ as a function of pore diameter as seen in Figure 1a, for higher fluid-to-solid ratios, the relaxation times were closer to each other. That means the confined molecules had enough degree of motional freedom. However, the confinement effect by the pore size was more pronounced in the case of the lowest fluid-to-solid ratio of 50 mg of either of

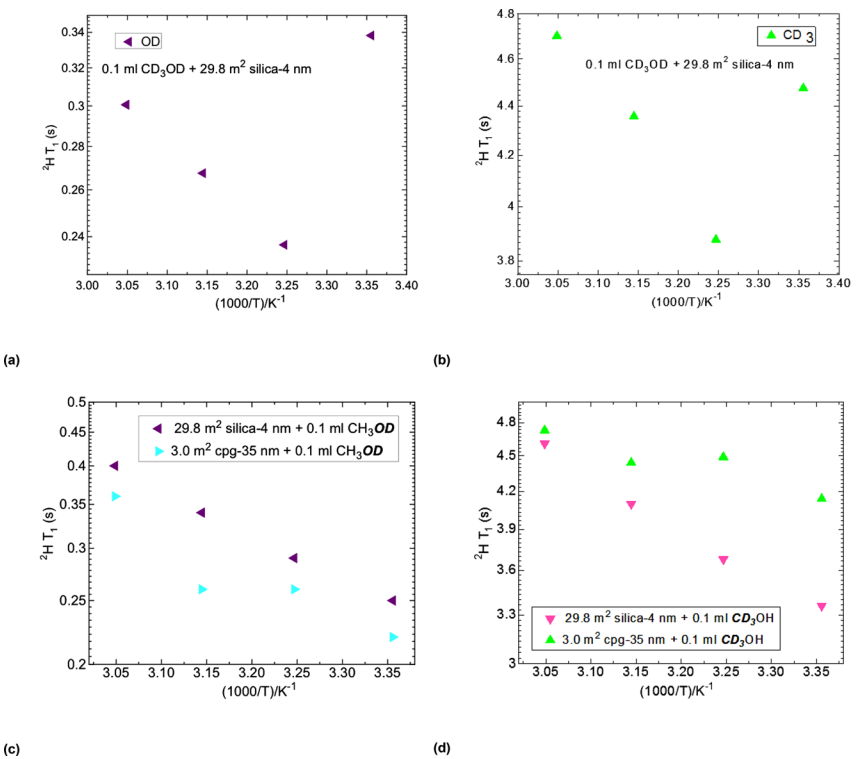


**Figure 2:** (a–d): Deuteron longitudinal relaxation time ($^2$H-$T_1$) of –OD (a) and $-CD_3$ (b) in mixtures of $CD_3OD$ with nanoporous silica. $^2$H-$T_1$ results of partially deuterated methanol $CH_3$***OD*** (c), and ***CD***$_3$OH (d) with the same fluid-to-solid ratio of 0.10 ml/0.050 g as a function of temperature at 298 K, 308 K, 318 K, and 328 K and pore diameters of 4 and 35 nm.

the porous matrix systems and 0.05 ml of low viscous fluid. There are two important points regarding the relaxation of the –OD. The –OD longitudinal relaxation time ($^2$H-$T_1$) in mixtures with cpg-35 nm did not reach values lower than 0.1 s for the temperature range studied. However, the –OD longitudinal relaxation time ($^2$H-$T_1$) was less than 0.1 s when $CH_3OD$ is confined into silica-4 nm. The second issue was about the degree of the relative deviation of longitudinal relaxation time as the fluid-to-solid ratio was decreased. The relative deviation was 2.5 fold for $–CD_3$ while it was fivefold for –OD (Figure 3c and d). For $–CD_3$, the $^2$H-$T_1$ values started decreasing from 5.0 s range in mixtures with cpg-35 nm, and reached the range around 2.5 s. However, the $^2$H-$T_1$ values of –OD started decreasing from 0.4 s range and reached the range around 0.08 s. The decrease in the $^2$H-$T_1$ values of –OD became stronger in mixtures with nanoporous silica. It seems that –OD interacts with oxygen of the OH on the pore walls. In this way, the possible O–D···O interaction is formed reducing the relaxation times. This indicates that in addition

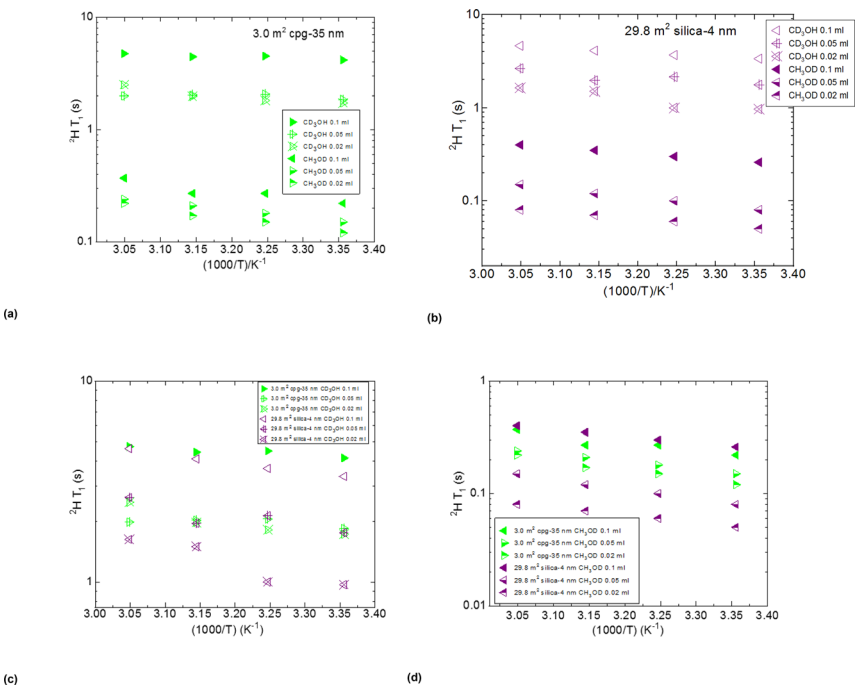


**Figure 3:** (a–d): Deuteron longitudinal relaxation time ($^2$H-$T_1$) of $CD_3OH$ and $CH_3OD$ in mixtures with cpg-35 nm, silica-4 nm as a function of temperature at 298, 308, 318, and 328 K, pore diameter of nanoporous matrix system, fluid-to-solid ratios of 0.10 ml/0.050 g, 0.05 ml/0.050 g, 0.02 ml/0.050 g, and fluid chemistry (switching from $CH_3OD$ to $CD_3OH$).

to confinement effect, there was a strong contribution of interactions arising from the nature of both the fluid and the matrix system. We also suggest that the other factor contributing to the discrepancy is the additional spectral density due to methyl ($-CD_3$) group orientation. The orientation of $-CD_3$ is relatively faster than that of $-OD$ because $-CD_3$ does not interact with $-OH$ of the silica pore wall.

Sattig et al. studied temperature-dependent rotational motion of supercooled $H_2O$ in MCM-41 type silica pores with diameters of 2.14, 2.76, and 2.93 nm by using $^2H$ NMR [41]. Sattig et al. observed a first kink in the temperature reliance accompanied by a solidification of a portion of the confined $H_2O$. This implied an alteration from bulk-like to interface-dominated water dynamics instead of a liquid-liquid phase transition. In the temperature range above 225 K, the confinement effect was observed. Above 225 K, the temperature reliance of $H_2O$ reorientation was weaker in the smaller pores, and in the bigger nanopores bulk-like water behavior was observed. Although controlled pore glass utilized in the present report has much larger pore diameter than the pore diameters of MCM-41 derivatives utilized in the study by Sattig et al. water confined into cpg-35 nm still showed deviation from bulk behavior [41]. For this reason, we suggest that the disordered structure of cpg-35 nm influences the dynamics of $H_2O$ leading to deviation from bulk behavior. Near 225 K, longitudinal magnetization relaxation ($T_1$) times for the ice in silica-2.1 nm confinement became too long for a dependable determination, while $T_1$ times for confined water in liquid state passes a minimum, showing that confined $H_2O$ has correlation times $\tau \approx 1/\omega_0 \approx 1$ ns. For the interpretation of the relaxation experiments, we consider Eq. (1). We expect a distribution of correlation times so that Eq. (2) of Supplementary Information based on the BPP (Bloembergen–Purcell–Pound) theory of relaxation does not apply. Rather, Eq. (1) is one way to consider this effect, assuming a bimodal distribution. In analyzing and explaining the longitudinal relaxation data obtained, we refer to Eq. (1) described below. We first consider a cylindrical pore with radius $R$ and length $l$, completely filled with water molecules shown with schematic in Figure 4. Due to confinement within the pores, the water molecules at the surface will experience a restricted motion with respect to the bulk like water at the center of pore. We assume that the water molecules within a distance $a$ from the surface are affected by the surface and the rest acts as bulk like water. Under these assumptions the observed proton relaxation time constant $T_{1,\text{observed}}$ will have a weighted average from water molecules near the surface and bulk like water molecules, where the weights are proportional to the volume [42, 43]. The number of protons/water molecules at the surface and in bulk-like state is proportional to the $V_{\text{Surface}}$ and $V_{\text{Bulk}}$, respectively. Thus, the observed $T_1$ relaxation can be explained by the following equation:

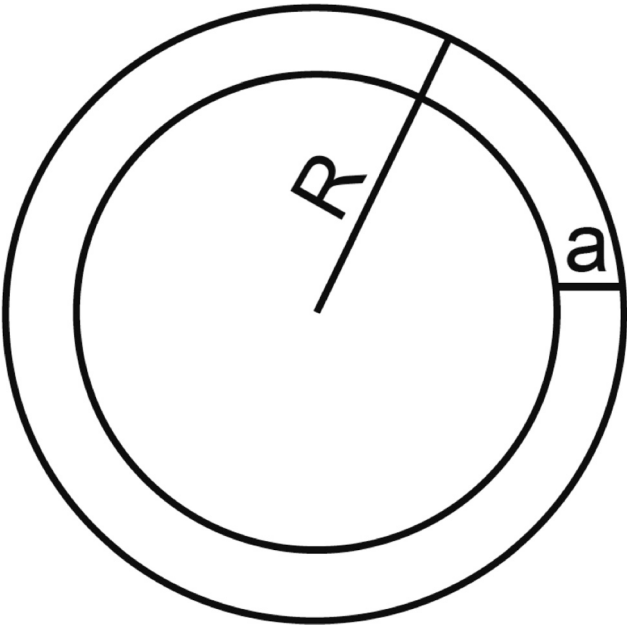


**Figure 4:** Schematic representation of a cylindrical pore with radius *R* and length *l*, completely filled with water molecules.

$$\left(1/T_{1,\text{observed}}\right) = (2a/R)\left[1/T_{1,\text{surface}} - 1/T_{1,\text{bulk}}\right] + \left[1/T_{1,\text{bulk}}\right] \quad (1)$$

where the equation assumes $a << R$.

This equation assumes an ideal case where the pores are totally filled with the fluid of interest. In our case, there is gradual increase in the amount of fluid mixed with the porous systems. This increases the amount of confined fluid. $T_{1,\text{surface}}$ values are calculated for the samples with the following volumes: 0.20 ml; 0.10 ml; 0.05 ml; 0.02 ml in 50 mg silica-4.0 nm (third set of samples identified in Table 1a), and by assuming 0.25 nm wall thickness, and taking 10 s of $T_1$ time for $D_2O$ in bulk referring to a recent paper on NMR relaxation times of residual water in $D_2O$ at high temperatures [44]. $T_{1,\text{surface}}$ values decrease as the wetting degree decreases from 0.040 to 0.031 s, and 0.032 to 0.028 s for the four mixtures mentioned above, respectively. This demonstrates that at lower wetting degrees, water layers strongly interact with the –OH groups of the pore walls.

In the case where volumes of 0.20 and 0.10 ml fluid (water) were confined into nanoporous silica-4.0 nm, there is excess water. However, excess water is still in interaction with the outside surface of nanoporous silica, and most likely moving in and out of the nanopores. Therefore, excess water does not show

distinguishable $T_1$ values. As a result, we suggest that the whole relaxation behavior can be traced back to the slowdown of interfacial water, and the observations can be rationalized by different ratios of interfacial to bulk-like water fractions as a function of temperature, and for various pore sizes and fillings.

Sattig et al. suggested that $^2$H NMR line-shape analysis evidenced pronounced dynamical heterogeneities for confined $H_2O$ [41]. However, in our study we did not conduct line-shape analysis; rather focus on $T_1$ and diffusion measurements at high temperatures. In another study on characteristic properties of $H_2O$ dynamical motions in confined geometries explored by quasi-elastic neutron scattering, Osti et al. mentioned primary single parameter $\theta$, which is the ratio between the average number of water molecules mostly affected by pore walls and the total number of $H_2O$ molecules under confinement [45]. If we consider $\theta$ as equal to a constant value such as $(X)$ for a complete saturation with and without excess water by taking filling mechanism of MCM-41 with $H_2O$ mentioned by Grünberg et al. [27] into account, we suggest that there are both $\theta \approx X$ and $\theta \leq X$ where there is dynamic exchange between confined water molecules (the ones not interacting with the pore walls) and the bulk excess water. For the samples with excess fluid as in the case of silica-4 nm, $\theta$ for different fluid–solid-ratios is equal to each other. When the fluid-to-solid ratio is decreased for the partially filled samples, $\theta$ also decreases down. Because $\theta$ is utilized for the slit-type, cylindrical, and spherical geometries, we do not apply $\theta$ in the case of confining water molecules into cpg-35 nm engineered system.

Annealing porous silicon between 300 and 600 °C induces structural changes [46]. Thermal treatment in the temperature range of 400–900 °C in vacuum formed oxidation and subsequent formation of a $SiO_2$ layer [47, 48]. For this reason, $T_1$ measurements of $D_2O$ in mixtures with porous systems were repeated while cooling down the samples in order to test any structural changes such as collapse of the pores at elevated temperatures. Table 2 lists the results. During cooling process, the $T_1$ values were measured again at 60 and 25 °C. The first values were reproducible which indicates that for the temperature range of the current study the porous systems did not undergo any significant structural changes.

The influence of nanopore size on the behavior of $D_2O$ was also tested. The surface area of cpg-35 nm and silica-4 nm are different (Supplementary Table S1). For this reason, the same amount of substrate was used and the $T_1$ values of $D_2O$ by varying the nanopore size for the same amount of fluid, 0.07 ml were compared. Figure 5 shows the comparison. At both lower and higher temperatures, the relaxation values of $D_2O$ were higher in the case of cpg-35 nm. This shows that there was confinement effect reducing the mobility of $D_2O$ molecules relatively stronger upon confining into the pores of silica system with narrower pore diameter. This allows comparison of relaxation independent of surface area but with different

**Table 2:** Reversibility of $T_1$ results obtained as a function of varying temperature to check the possible deformation of the pores at elevated temperatures.

| Temperature (°C) | 29.8 $m^2$ silica-4 nm + 0.1 ml $D_2O$ | |
|---|---|---|
| | $^2$H-$T_1$ (s)[a] | Reversibility ($^2$H-$T_1$ (s))[b] |
| 25 | 0.24 | 0.37 |
| 60 | 0.75 | 0.77 |
| **Temperature (°C)** | **3.0 $m^2$ cpg-35 nm + 0.1 ml $D_2O$** | |
| | $^2$H-$T_1$ (s)[a] | Reversibility ($^2$H $T_1$ (s))[b] |
| 25 | 0.39 | 0.40 |
| 60 | 0.83 | 0.83 |

[a]Measurement performed while increasing the temperature.
[b]Measurement performed while decreasing the temperature.

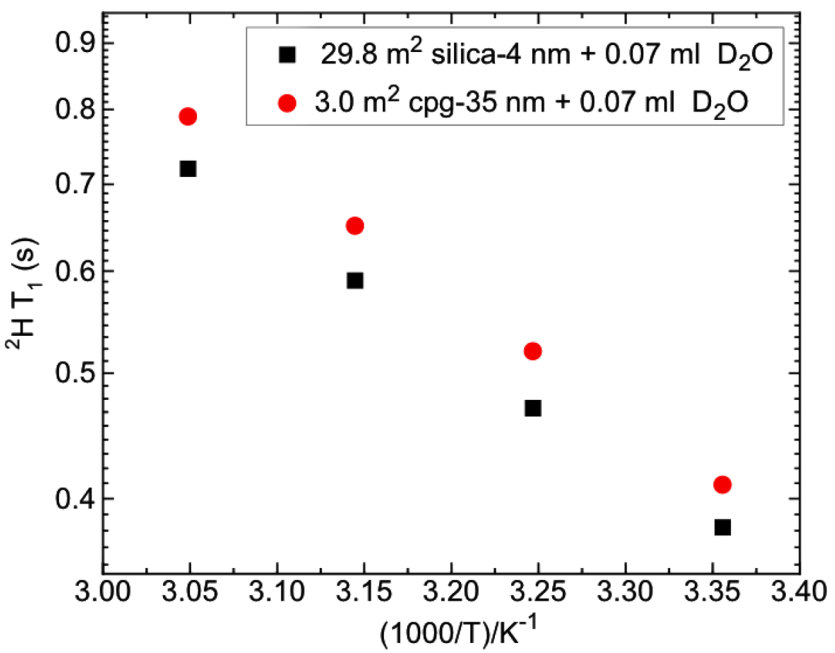


**Figure 5:** Deuteron longitudinal relaxation time ($^2$H-$T_1$) results obtained as a function of pore diameters of 4 and 35 nm, and temperature at 298, 308, 318, and 328 K where 0.07 ml $D_2O$ is confined into 50 mg of either porous silica-4 nm or cpg-35 nm.

nanopore size. This was used as discussed below for conducting high-pressure NMR experiments of confined low viscous fluids by varying pore size. As the temperature was increased, the relaxation values became higher.

## 3.2 Dynamics of confined fluids under pressure

Dynamics of methanol and propanol have been studied in pure state by high-pressure NMR [49, 50]. Methanol was considered as an ideal molecule for exploring hydrogen bonding in the liquid state. Methanol has been studied up to 3.5 kbar by NMR [49, 51] and up to 20 kbar by Raman scattering [52], while dynamics of isopropanol was studied up to 3 GPa [50]. Studying pure methanol by high-pressure NMR revealed shortening in hydrogen bond distances induced by pressure. There was also an increase in the hydrogen-bonding network of methanol observed when pressure was increased at constant temperature [51, 53]. Stronger hydrogen bonding at elevated pressures in the liquid state might kinetically obstruct structural reordering [49]. This led to shorter $T_1$ values, indicative of slow molecular tumbling. Dynamics of $H_2O$ at high-pressures were studied both in bulk and in hydrated Nafion [54, 55]. The first coordination shell of liquid $H_2O$ is unperturbed by compression [54].

Figure 6a and b exhibits longitudinal relaxation of deuterated methanol and $D_2O$ in bulk and in mixtures with nanoporous proxies by varying high-pressure and various solid-to-fluid ratios. The deviation of longitudinal relaxation times from bulk liquid upon confinement was independent of chemistry of the fluid. In the case of controlled size pore glass; the relaxation values of both of the fluids were closer to these of the bulk values. Further, as the solid-to-fluid ratio was lowered, the deviation became larger. The longitudinal relaxation of $D_2O$ remained unperturbed by compression [53]. This result was independent of being in either pure or confined state. Moreover, in bulk there was approximately 30% decrease in $T_1$ value of $CD_3OD$ as pressure was increased, while such a decrease in $T_1$ values under high pressure was not observed when $CD_3OD$ was confined into the nanoporous proxies (Figure 6b). This shows that $CD_3OD$ is slightly compressed under high pressure in bulk but not in the confined state. Further, the $T_1$ times of $CD_3OD$ are longer than that of $D_2O$ in both bulk and confined states. Internal rotation of the $-CD_3$ group is faster than the $-OD$ group rotation, in turn leading to longer $T_1$ times of $CD_3OD$ compared to that of $D_2O$ [31]. The insignificant change in $T_1$ values of both $D_2O$ and $CD_3OD$ in bulk as well as the confined fluid is also explained by an insignificant change in density of the fluids. This insignificant change in density arises from a possible controversial "balance" between a shortening in diameter of O–D bond ($r_{O-D}$) leading to a strengthening of hydrogen bond and an increase in

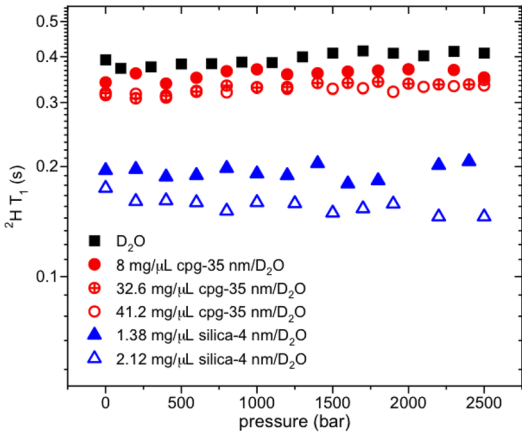


(a)

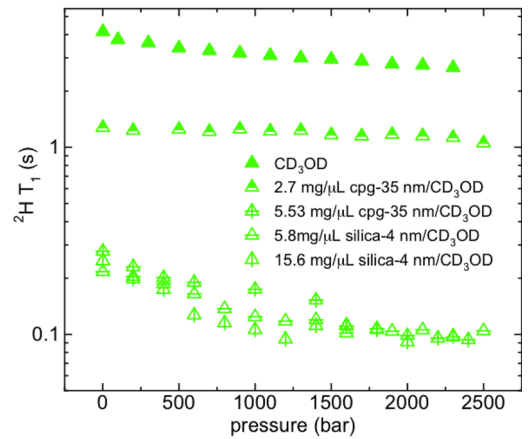


(b)

**Figure 6:** (a, b): Deuteron longitudinal relaxation time ($^2$H-$T_1$) of $D_2O$ (a) and $CD_3OD$ (b) in pure state and in mixtures with silica-4 nm, cpg-35 nm as a function of pressure from 0 to 2500 bar, pore diameter of nanoporous matrix system, fluid-to-solid ratio, and fluid chemistry.

frequency of –OD vibration ($\nu_{O-D}$) thus weakening the hydrogen bonding [56]. Hence, the pore walls impose a restricted geometry lowering the $T_1$ values and slowing the dynamics of confined fluids compared to the bulk, while the density of confined fluids changed little as the pressure was increased. The slight change in $T_1$ times of $CD_3OD$ in bulk is also attributed to the faster rotational behavior of $-CD_3$

with respect to that of –OD forming a network type structure disturbed by confinement.

The quadrupolar interaction in the deuteron is sensitive to the properties of the chemical bond such as the bond length. The deuteron NMR spectra helped with investigating molecular mobility because of the high value of the quadrupole coupling constant ($Q_{CC}$) [57, 58]. $Q_{CC}$ might change by pressure and temperature [33, 59]. In the case of $D_2O$ confinement, the bond length in O–D···O network was not affected by pressure. Further, applying high pressure did not alter the quadrupolar constant. It has been suggested that pressure has a minor effect on the degree of hydrogen bonding. The $Q_{CC}$ decreased qualitatively arising from shortening in bond length in $CD_3$–O–D···O network of $CD_3OD$ [42]. In the mixtures, there was combined effect of confinement and increasing strength in hydrogen bonding. The combination was indicated even in the case of cpg-35 nm system with larger pores. For instance, with the ratio of 5.53 mg/μl (cpg-35 nm/fluid) the relaxation value approached to these with the fluid confined into mesoporous silica with smaller pores. In analyzing and explaining the longitudinal relaxation data obtained under high-pressure, we refer again to Eq. (1) explained above. However, the pores were still not completely saturated with the fluid. For this reason, this equation is not applicable in terms of differentiating between "surface" water and confined but "bulk like" water. In other words, the fraction of liquid in contact of the pore surface was high due to non-complete filling of the pores. The observed $T_1$ is attributed primarily to that fraction.

## 3.3 Diffusion of water and methanol

Figure 7a shows diffusion coefficients of water as a function of fluid-to-solid ratio [60]. Note diffusion of fluid molecules between nanoparticles is probed by taking into account the fact that the diffusion attitude heavily relies on the rates of exit/re-entrance into the nano-pores and the motion between the particles. In addition, the confined molecules in the mixtures with silica-4.0 nm are constrained to move in only one direction (anisotropically), so in a two-dimensional structure, and in the case of cpg-35 nm a disordered statistical distribution of motion for the confined fluids is valid.

Moreover, the diffusion measurements probe displacements on the order of tens of micrometers, which are much larger than both the sizes and the pore diameter of the mesoporous silica particles-200 and 4 nm, respectively, hence the probed diffusion is anisotropic. Therefore, restricted/anisotropic diffusion is considered in explaining the results [61]. We should expect diffusion of water in two-dimensional (2D) morphology in both of the confined matrixes: silica-4 nm

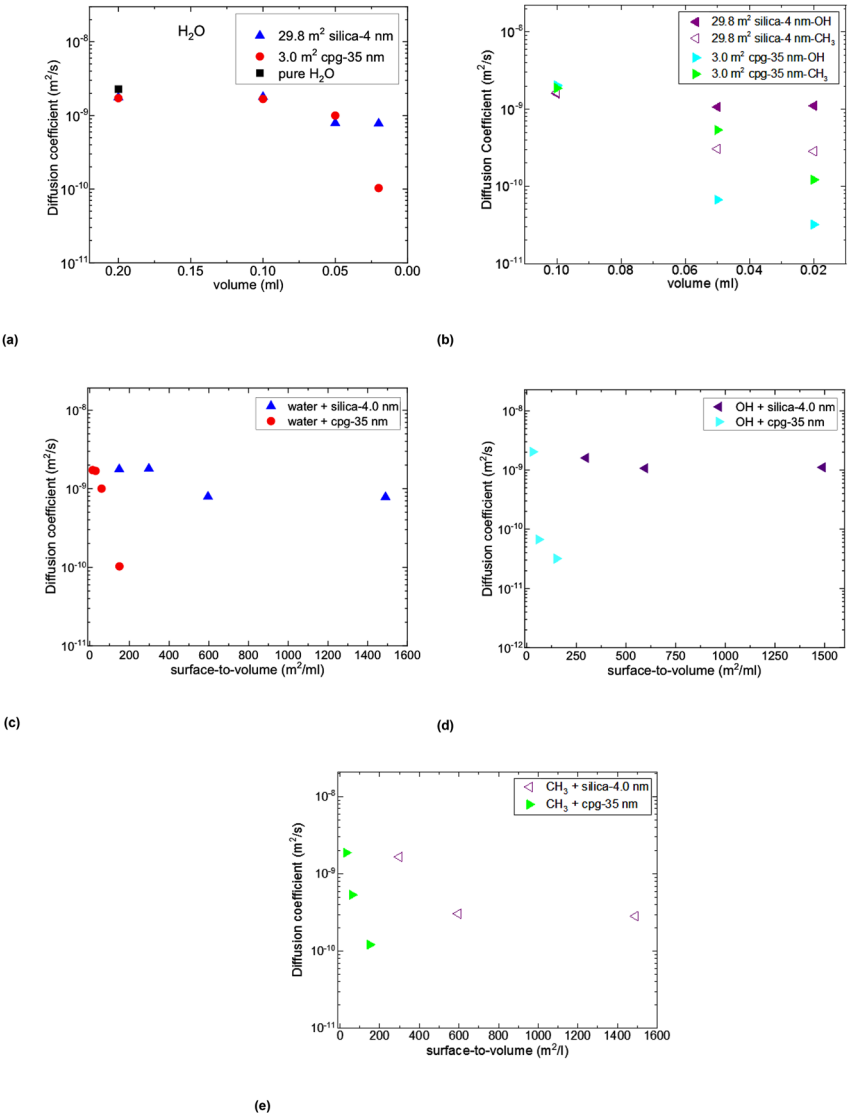


**Figure 7:** (a–e): (a) Diffusion coefficient of water in pure state and mixtures with silica-4 nm and cpg-35 nm as a function of volume at 298 K and where the amount of solid is 0.050 g. The diffusion coefficient value of water in pure state is taken from ref. [53]. (b) Diffusion coefficient of methanol (–$CH_3$ and –OH) in mixtures with silica-4 nm and cpg-35 nm as a function of volume at 298 K and where the amount of solid is 0.050 g. (c) Diffusion coefficient of water in mixtures with silica-4 nm acquired at 298 K as a function of solid surface to fluid volume ratio (c). Diffusion coefficient of methanol (–$CH_3$ and –OH) in mixtures with silica-4 nm (d) and cpg-35 nm (e) acquired at 298 K as a function of solid surface to fluid volume ratio.

and cpg-35 nm. According to Stallmach et al. [61], there are two morphological possibilities restricting diffusion of the confined fluid: (i) permeable pore walls, and (ii) impenetrable pore walls where a water molecule moving in the channel axis has a chance to change its direction by either hopping from one channel to the neighbor one or continuing its diffusion in one channel that is slightly bent into another path. In either possibility, the fluid diffuses anisotropically. In addition, regarding motion of water in cpg-35 nm, we suggest that there is random distribution of diffusion of confined fluids. As shown in Figure 7, when the volume of confined fluid was decreased, diffusion coefficient also decreased. The lowest diffusion coefficient value was determined in the sample of 0.25 ml water confined into cpg-35 nm. As argued by Stallmach et al. [61], diffusion in parallel or perpendicular to the matrix axis or even when the channel is bent so random orientation of the host matrix deviates from the bulk behavior. The current results clearly present that the deviation in the measured diffusion of confined fluids with respect to their corresponding bulk is influenced by the host matrix, and whether the matrix shows regularity or randomness in its morphology. Moreover, in the case of heterogeneous samples such as the nanoporous silica, the measured diffusion could be shorter than the real diffusion [62]. However, as mentioned in the experimental section, stimulated echo pulse sequence is utilized in the present study in order to eliminate this problem [10]. Therefore, we consider a model free of isotropic diffusion while extracting the diffusion coefficient values.

The decrease in water diffusion coefficient was approximately independent of pore size, as expected. The diffusion coefficient values were in the same range, when the porous systems are filled with either 0.2 ml or 0.1 ml of water. In other words, we switch to heterogeneous systems of partial filling of the pores without excess water as the fluid-to-solid ratio is decreased. When the volume of fluid mixed with the mesoporous system was below 0.1 ml, deviation from bulk liquid state was more pronounced. The confinement effect leads to restriction in motion. The diffusion coefficient values are average values of water molecules with either two or three different environments: (i) bulk-like water interacting with the outer surface of the porous systems if there is any excess fluid, (ii) trapped water within porous matrix system but diffuse anisotropically, (iii) water molecules interacting with the interface of the mesoporous systems. The diffusion coefficient values of methanol in porous medium are shown in Figure 7b. Diffusion coefficient decreases as the fluid-to-solid ratio is decreased. When the volume of methanol in mixtures with porous systems was 0.1 ml, the diffusion coefficient values were slightly higher in the mixture with cpg-35 nm having larger pore size. When either 0.05 ml or 0.02 ml of methanol was mixed with cpg-35 nm, at first we thought that $-CH_3$ had higher diffusion coefficients than –OH. On the contrary, for the volumes of either 0.05 ml or 0.02 ml methanol in porous silica-4 nm, it was suggested that –OH

had higher diffusion coefficient values than these of $-CH_3$. The diffusion coefficient values did not change significantly when the amount of confined fluid was lowered. Comparison of diffusion coefficient values for the mixtures with 0.02 ml methanol demonstrated higher diffusion coefficient value for porous silica-4 nm. We can ask whether different portions of the same molecule might exhibit different diffusion coefficients when the molecules diffuse as an entity. For this reason, we suggest that the observed differences in diffusion coefficients of $-CH_3$ and $-OH$ imply proton transport independent of molecular movement. Specifically, Grotthuss-type motion could contribute to the results of $-OH$ in the case of $CH_3OH$. According to Grotthuss mechanism of motion, a proton moves via the hydrogen bonding networks, where both proton transfer and sequential molecular rotation occur simultaneously. Proton transfer of $-OH$ in chains of hydrogen-bonded methanol molecules, consistent with Grotthuss-type motion, might produce two different diffusion coefficients [63].

In the report by D'Agostino et al., diffusion coefficients of various alkanes and polyols within mesoporous materials were measured, and it was found that polyols showed enhanced diffusivity within the pores with respect to alkanes [3]. This was attributed to disruption in hydrogen bonding network of polyols within the pores [3]. We suggest that for the lowest fluid-to-solid ratio in silica-4 nm with narrower pores, the hydrogen-bonding network was disrupted. Due to this disruption, the diffusion coefficient of methanol was higher in the mixture with silica-4 nm compared to the mixture with cpg-35 nm.

To explore this further we examined the diffusion coefficient data as a function of solid surface area to fluid volume ratio. Keeping the solid surface area constant and lowering the volume of fluid, increases the surface to volume ratio. As seen in Figure 7c, when this ratio decreases from 1500 to 600 $m^2$/ml, the diffusion coefficient of water did not change, so reaching a plateau. Considering the filling mechanism of the pores of silica-4 nm with water suggested by Grünberg et al. [27], we believe that first monolayers are formed on the pore walls by strong interaction with $-OH$, which already decorates the pore walls. There was an increase in the diffusion coefficient value of water in mixtures with silica-4 nm, as the solid surface area to fluid volume ratio decreased. This increase is attributed to the contribution of water confined but free within the pores to the average diffusion coefficient. Such a plateau at higher solid surface area to fluid volume ratio is not observed in the case of water confined into the pores of cpg-35 nm. More interestingly, at lower filing ratios (higher solid surface area to fluid volume), diffusion coefficient of water in cpg-35 nm is lower than that of water confined into silica-4 nm with narrower pores. We suggest that this result arises from disruption of hydrogen bond network of water confined into cpg-35 nm [3]. It appears that diffusion coefficients for both $H_2O$ and $CH_3OH$ feature a substantial drop in a silica-

4 nm matrix. Moreover, it is noteworthy that cpg-35 nm was not investigated for higher surface to volume ($S/V$) ratios. In the case of $CH_3OH$, we consider diffusion of –OH and $-CH_3$ in silica-4 nm and cpg-35 nm separately as shown in Figure 7d and e. Diffusion coefficient of –OH in silica-4 nm reaches a plateau, as solid surface area to fluid volume ratio was increased, while that of –OH in cpg-35 nm showed reduction as the ratio was increased. Diffusion coefficients of –OH in cpg-35 nm were much lower than those of in silica-4 nm. This is a similar behavior to that of $H_2O$ diffusion in silica-4 nm and cpg-35 nm. For this reason, we suggest that disruption of hydrogen bonding ability exists due to the geometry of the porous materials. Moreover, diffusion coefficient values of sub-molecular functional groups with hydrogen bonding ability such as –OH are influenced by the nano-confined geometry. This is independent of varying fluid chemistry from 2 –OH ($H_2O$) to 1 –OH ($CH_3OH$). Whereas, diffusion coefficient values of $-CH_3$ in silica-4 nm also reached a plateau as the solid surface to fluid volume ratio was increased. Diffusion coefficient values of $-CH_3$ in cpg-35 nm showed a decreasing trend as the solid surface to fluid volume ratio was decreased. However, diffusion coefficient values of $-CH_3$ did not show significant change when the confined geometry was varied from straight channels of silica-4 nm to irregular pores of cpg-35 nm. This shows that $-CH_3$ diffusion is affected less by the geometry of the nanoporous matrix system. Deviations in diffusion coefficients of confined fluids with respect to pure bulk state indicate that in addition to confinement effect, possible specific interactions with the pore walls such as hydrogen bonding and disruption of them, as well as nanopore geometry influence the diffusion behavior of confined fluids. Rather than pore diameter, solid surface to fluid volume ratio is another important factor affecting the diffusion behavior in confined state of matter.

Grünberg et al., studied behavior of water confined into mesoporous silica of MCM-41 and SBA-15 types with two-dimensional hexagonal arrays of cylindrical pores of identical size ranging from 2 to 10 nm [27]. Because of the highly dense pores and comparatively small pore diameters, these nanoporous silica proxies show larger inner surfaces with respect to the volume of the single pore. There is a favored axis along the cylinder axis of the pores arising from highly anisotropic geometry of the pores. Diffusion of fluid in silica-4 nm with parallel-aligned pores resembling the structure of MCM-41 is considered to be orientation-dependent so shows anisotropy. Thus, diffusion of molecules deviates from bulk [64]. Cpg-35 does not indicate any periodicity as shown in the representative SEM image as shown in Figure 1c. Non-periodicity of the cpg-35 nm structure does not allow proper modeling of the filling mechanism of the controlled pore glass pores. The disordered structure of cpg-35 nm also disrupts the hydrogen-bonding network due to heterogeneity in the morphology of the porous structure as discussed by

D'Agostino et al. [3]. In addition, Grünberg et al. considered possible –OH groups in the mixtures of water and silica proxies and corresponding NMR resonances in ppm. For instance, when water is confined into SBA-15, the first monomolecular water layer is formed at a $H_2O$ content of 8% [27]. There are $^1$H NMR signals solely for a defined structure of the water molecules interacting with the pore wall and the other molecules [27, 65]. Practically speaking, dynamic exchange can influence behavior such as molecular reorientations of the water molecules. Rotations of the surface –OH groups in general will cause variations in the spectral positions of these chemical shifts leading to absolute or full averaging of the isotropical chemical shift positions [64]. This is taken into account in our analysis of the confined fluid dynamics with excess amount of water. For this reason, we think of average chemical shifts involving various hydrogen-bonding scenarios. We suggest that this leads to average diffusion coefficients and relaxation times.

# 4 Conclusion

This study applied state-of-the-art characterization methods (e.g., SEM, TEM) to assess two nanoporous silica matrices and in situ NMR spectroscopy to probe the dynamics of two hydrogen-bonded fluids, water and methanol, in nanopores as a function of pore features temperature, pressure and fluid/solid ratio. The materials have different pore size, volume and distribution with resulting different surface area to volume ratios. The silica-4.0 nm and cpg-35 nm both exhibit –OH decoration on their pore walls, and the cpg-35 nm exhibits disordered morphology compared to the more ordered well-aligned pores in the MCM-41 silica. These two nanoporous silicas are typically used as sorbents and catalytic supports but they also can be considered reasonable proxies for porous earth materials.

The specific goals of the study were to study relaxation and diffusion behavior of fluids under confinement relevant to geochemically relevant conditions of high-temperature and high-pressure. The selected fluids were water, methanol, and their deuterated forms because of their hydrogen bonding capability. Mesoporous silica and controlled pore glass were the host matrixes utilized for confining the fluids after characterizing the porous matrixes with the advanced techniques. The thermal stability of the mesoporous silica was also tested.

First, the diffusion and relaxation behavior of both fluids in the confined state exhibit deviation from bulk fluids as the fluid-to-solid ratio was decreased. Relaxation measurements were conducted by ramped temperature up and down, and revealed that nanoporous materials were stable over the temperature range studied. Deviation of dynamical behavior of confined fluids from that of bulk fluid is observed also under high-pressure. Variable pressure deuteron NMR relaxation

of confined $D_2O$ and $CD_3OD$ demonstarted that $D_2O$ is not compressible under the current high-pressure conditions (up to 2.5 kb) even in confined state. The compressibility of $CD_3OD$ by high-pressure is insignificant as revealed by $^2H$ $T_1$ NMR measurements. In the confined state, pressure has a minimal influence on dynamics of both of the fluids. The results clearly indicate that the hydrogen-bonding network in nanoconfinement was affected by temperature largely but essentially pressure-independent. The current findings demonstrate that NMR methods are beneficial in gaining insights into the physical chemistry of confined fluids. Moreover, silica based nanoporous engineered materials can act as reasonable proxies for heterogeneous subsurface materials suitable for confining crude oil and brine solutions to mimic nano-environments present in natural systems such as rocks common to oil reservoirs.

**Acknowledgment:** Support for S. Ok was provided by the A.P. Sloan Foundation sponsored Deep Carbon Observatory. DRC, JS and SW were supported by the Department of Energy, Basic Energy Sciences Geosciences Program under grant DE-SC0006878. The authors are also thankful to the anonymous reviewers for their suggestions at different stages of the manuscript.

**Author contribution**: All the authors have accepted responsibility for the entire content of this submitted manuscript and approved submission.

**Research funding**: Support for S. Ok was provided by the A.P. Sloan Foundation sponsored Deep Carbon Observatory. DRC, JS and SW were supported by the Department of Energy, Basic Energy Sciences Geosciences Program under grant DE-SC0006878. The authors are also thankful to the anonymous reviewers for their suggestions at different stages of the manuscript.

**Conflict of interest statement**: The authors declare no conflicts of interest regarding this article.

# References

1. Millischuk A. A., Ladanyi B. M. *J. Chem. Phys.* 2014, *141*, 18C513..
2. Vogel M. *Eur. Phys. J.* 2010, *189*, 47.
3. D'Agostino C., Mitchell J., Gladden L. F., Mantle M. D. *J. Phys. Chem. C* 2012, *116*, 8975.
4. Demuth D., Sattig M., Steinrucken E., Weigler M., Vogel M. *Z. Phys. Chem.* 2018, *232*, 1059.
5. Gelb L. D., Gubbins K. E., Radhakrishnan R., Sliwinska-Bartkowiak M. *Rep. Prog. Phys.* 1999, *62*, 1573.
6. Stallmach F., Graser A., Karger J., Krause C., Jeschke M., Oberhagemann U., Spange S. *Micropor. Mesopor. Mat.* 2001, *44*, 745.

7. Cole D. R, Mamontov E., Rother G. Neutron applications in earth, energy and environmental sciences. In *Neutron Scattering Applications and Techniques*; Liang L., Rinaldi R., Schober H., Eds. Springer: Boston, 2009; pp. 547–570.
8. Cole D. R., Herwig K., Mamontov E., Larese L. Z. *Rev. Mineral. Geochem.* 2006, *63*, 313.
9. Webber B., Dore J. *J. Phys. Condens. Matter* 2004, *16*, S5449.
10. Gautam S. S., Ok S., Cole D. R. *Front. Earth Sci.* 2017, *5*, 49.
11. Packer K. J. *Magn. Reson. Imaging* 2003, *21*, 163.
12. Song Y.-Q. *Cement Concrete Res*. 2007, *37*, 325.
13. Kittler W. C., Obruchkov S., Galvosas P., Hunter M. W. *J. Magn. Reson.* 2014, *247*, 42.
14. D'Orazio F., Bhattaharja S., Halperin W. P., Gerhardt R.*Phys. Rev. B* 1990, *42*, 6503.
15. D'Orazio F., Bhattaharja S., Halperin W. P., Eguchi K., Mizusaki T. *Phys. Rev. B* 1990, *42*, 9810.
16. Bhattachrja S., D'Orazio F., Tarczon J. C., Halperin W. P. *J. Am. Ceram. Soc.* 1989, *72*, 2126.
17. Sindorf D.W., Maciel G. E. *J. Am. Chem. Soc.* 1983, *105*, 1487.
18. Brodrecht M., Kumari B., Breitzke H., Gutmann T., Buntkowsky G. *Z. Phys. Chem.* 2018, *232*, 1127.
19. Milischuk A. A., Ladanyi B. M. *J. Chem. Phys.* 2011, *135*, 174709.
20. Bianco V., Franzese G. *Sci. Rep.* 2014, *4*, 4440–4441.
21. Paul D. R. *Science* 2012, *335*, 413.
22. Zhang Y., Faraone A., Kamitakahara W. A., Liu K. H., Mou C. Y., Leao J. B., Chang S., Chen S. H. *Proc. Natl. Acad. Sci. USA* 2011, *108*, 12206.
23. Faraudo J., Bresme F. *Phys. Rev. Lett.* 2004, *92*, 236102.
24. Zangi R., Mark A. E. *Phys. Rev. Lett.* 2003, *91*, 025502.
25. Ruhle B., Davies M., Lebold T., Brauchle C., Bein T. *ACS Nano* 2012, *6*, 1948.
26. Zhao H., Chen Q., Zhang S. *Micropor. Mesopor. Mater.* 2012, *155*, 240.
27. Grünberg B., Emmler T., Gedat E., Shenderovich I., Findenegg G. H., Limbach H.-H., Buntkowsky G. *Chem. Eur. J.* 2004, *10*, 5689.
28. Corsaro C., Maisano R., Mallamace D., Dugo G. *Physica A* 2013, *392*, 596.
29. Inlow R. O., Joesten M. D., Van Wazer J. R. *J. Phys. Chem.* 1975, *79*, 2307.
30. Kleinberg R. L., Kenyon W. E., Mitra P. P. *J. Magn. Res. Ser. A* 1994, *108*, 206.
31. Versmold H. *Ber. Bunsenges. Phys. Chem.* 1980, *84*, 168.
32. Hansen E.W., Simon C., Haugsrud R., Raeder H., Bredesen R. *J. Phys. Chem. B.* 2002, *106*, 12396.
33. Lang E., Ludemann H.-D. *Ber. Bunsenges. Phys. Chem.* 1980, *84*, 462.
34. Stoch G., Ylinen E. E., Punkkinen M., Petelenz B., Birczynski A. *Solid State Nucl. Magn. Reson.* 2009, *35*, 180.
35. Lalowicz Z. T., Stoch G., Birczynski A., Punkkinen M., Ylinen E. E., Krzystyniak M., Gora-Marek K., Datka J. *Solid State Nucl. Magn. Reson.* 2012, *45–46*, 66.
36. Williams J. C., McDermott A. E. *J. Phys. Chem. B.* 1998, *102*, 6248.
37. Ueda T., Kurokawa K., Kawamura Y., Miyakubo K., Eguchi T. *J. Phys. Chem. C* 2012, *116*, 1012.
38. Angell C. A. *Science* 1995, *267*, 1924.
39. Angell C. A. *J. Non-Cryst. Solids* 1991, *131–133*, 13.
40. Bergman R., Swenson J. *Nature* 2000, *403*, 283.
41. Sattig M., Reutter S., Fujara F., Werner M., Buntkowsky G., Vogel M. *Phys. Chem. Chem. Phys.* 2014, *16*, 19229.
42. Gallegos D. P., D. M. Smith, C. J. Brinker. *J. Coll. Inter. Sci.* 1988, *124*, 186.
43. Timur A. *J. Petrol. Technol.* 1969, *21*, 775.
44. Koylu M. Z. *Int. J. Sci. Res.* 2018, *7*, 40.

45. Osti N. C., Cote A., Mamontov E., Ramirez-Cuesta A., Wesolowski D. J., Diallo S. O. *Chem. Phys.* 2016, *465–466*, 1.
46. Herino R., Perio A., Barla K., Bomchil G. *Mater. Lett.* 1984, *2*, 519.
47. Moller F., Ben Chorin M., Koch F. *Thin Solid Films* 1995, *255*, 16.
48. Hadj Z. N., Vergnat M., Delatour T., Burneau A., De Donato P., Barres O. *Thin Solid Films* 1995, *255*, 228.
49. Okuchi T., Cody G. D., Mao H.-K., Hemley R. J. *J. Chem. Phys.* 2005, *122*, 244509.
50. Hakes M., Zeidler M. D. *Phys. Chem. Chem. Phys.* 2002, *4*, 5119.
51. Bai S., Yonker C. R. *J. Phys. Chem. A* 1998, *102*, 8641.
52. Arencibia A., Taravillo M., Perez F.J., Nunez J., Baonza V. G. *Phys. Rev. Lett.* 2002, *89*, 195504.
53. Czeslik C., Jonas J. *Chem. Phys. Lett.* 1999, *302*, 633.
54. Soper A. K., Ricci M. A. *Phys. Rev. Lett.* 2000, *84*, 2881.
55. Greenbaum S., Jayakody J. R. P., Stallworth P. E., Mananga E., Zapata-Farrington J. *J. Phys. Chem. B* 2004, *108*, 4260.
56. Gorbaty Y. E., Bondarenko G. V., Kalinichev A. G., Okhulkov A. V. *Mol. Phys.* 1999, *96*, 1659.
57. Arnold M. R., Ludemann H.-D. *Phys. Chem. Chem. Phys.* 2002, *4*, 1581.
58. Lalowicz Z. T., Sotch G., Birczynski A., Punkkinen M., Krzystyniak M., Gora-Marek K., Datka J. *Solid State Nucl. Magn. Reson.* 2010, *37*, 91.
59. Lee Y. K., Campbell J. H., Jonas J. J. *Chem. Phys.* 1974, *60*, 3537.
60. Holz M., Weingartner H. *J. Magn. Reson.* 1991, *92*, 115.
61. Stallmach F., Karger J., Krause C., Jeschke M., Oberhagemann U. *J. Am. Chem. Soc.* 2000, *122*, 9237.
62. Cotts R. M. *J. Magn. Reson.* 1989, *83*, 252.
63. Lim D.-W., Sadakiyo M., Kitagawa H. *Chem. Sci.* 2019, *10*, 16.
64. Degat E., Schreiber A., Findenegg G., Shenderovich I., Limbach H.-H., Buntkowsky G. *Magn. Reson. Chem.* 2001, *39*, S149.
65. Buntkowsky G., Breitzke H., Adamczyk A., Roelofs F., Emmler T., Gedat E., Grünberg B., Xu Y., Limbach H.-H., Shenderovich I., Vyalikh A., Findenegg G. *Phys. Chem. Chem. Phys.* 2007, *9*, 4843.

**Supplementary Material:** Supplementary Material to this article can be found online at (https://doi.org/10.1515/ZPCH-2019-1510).